Abstract

Two fundamental facts of the modern wave turbulence theory are 1) existence of power energy spectra in k-space, and 2) existence of "gaps" in this spectra corresponding to the resonance clustering. Accordingly, three wave turbulent regimes are singled out: *kinetic*, described by wave kinetic equations and power energy spectra; *discrete*, characterized by resonance clustering; and *mesoscopic*, where both types of wave field time evolution coexist. In this paper we study integrable dynamics of resonance clusters appearing in discrete and mesoscopic wave turbulent regimes. Using a novel method based on the notion of dynamical invariant we establish that some of the frequently met clusters are integrable in quadratures for arbitrary initial conditions and some others – only for particular initial conditions. Integrable clusters yield pattern formation in kinetic and mesoscopic wave turbulent regimes.

PACS: 10.180,-a, 67.40.Hf, 68.03Kn, 68.03Hj

Key Words: Hamiltonian formulation, nonlinear resonance, NR-diagram, integrable dynamics

Corresponding author:

E. Kartashova,

Address: Altenbergerstr. 69, 4040 Linz, Austria;

Tel.: +43 732 2468 99 29, Fax: +43 732 2468 99 30,

E-mail: lena@risc.uni-linz.ac.at

Resonance clustering in wave turbulent regimes: Integrable dynamics

Elena Kartashova[†], Miguel D. Bustamante
lena@risc.uni-linz.ac.at, miguel.bustamante@ucd.ie
[†]J. Kepler University, Linz, Austria
[*]University College Dublin, Dublin, Ireland

February 26, 2010

1 Introduction

The broad structure of modern nonlinear science born at the edge of physics and mathematics includes an enormous number of applications in cosmology, biochemistry, electronics, optics, hydrodynamics, economics, neuroscience, etc. The emergence of nonlinear science itself as a collective interdisciplinary activity is due to the awareness that its dynamic concepts first observed and understood in one field (for example, population biology, flame-front propagation, non-linear optics or planetary motion) could be useful in others (such as in chemical dynamics, neuroscience, plasma confinement or weather prediction). The theory of integrable Hamiltonian systems, a generalization of the classical theory of differential equations, is the nucleus of the whole nonlinear science. Various classifications of integrable systems are presently known which turned out to be quite useful for physical applications, [26]. However, the notion of integrability itself is ambitious. There are many quite different definitions of integrability, for instance integrability in terms of elementary functions (equation $\ddot{y} = -y$ has the explicit solution $y = a\sin(x+b)$); integrability *modulo* class of functions (equation $\ddot{y} = f(y)$ has general solutions in terms of elliptic functions), etc. An example of less obvious definition of integrability is C-integrability, [4]: integrability *modulo* change of variables, meaning that a *nonlinear* equation is called C-integrable if it can be turned into a *linear* equation by an appropriate invertible change of variables. For instance, Thomas equation $\psi_{xy} + \alpha\psi_x + \beta\psi_y + \psi_x\psi_y = 0$

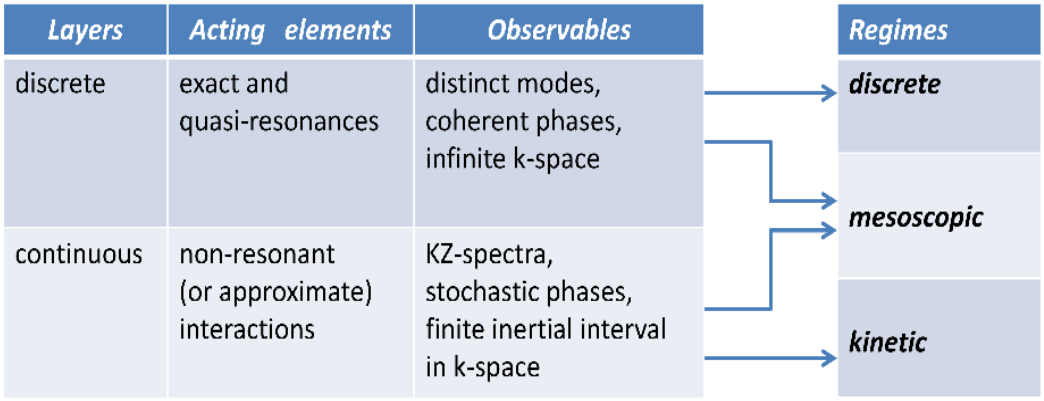

Figure 1: Color online. Schematic representation of wave turbulent regimes.

is C-integrable. In the present paper, all integrable dynamical systems have solutions that are written out *in quadratures*.

The dynamical systems we are interested in, describe nonlinear resonance clusters appearing in evolutionary dispersive PDEs in two space variables. Nonlinear resonances are ubiquitous in physics. They appear in a great amount of typical mechanical systems [22], in engineering [23], astronomy [21], biology [9], etc. etc. Euler equations, regarded with various boundary conditions and specific values of some parameters, describe an enormous number of nonlinear dispersive wave systems (capillary waves, surface water waves, atmospheric planetary waves, drift waves in plasma, etc.) all possessing nonlinear resonances.

The classical approach of statistical wave turbulence theory in a nonlinear wave system assumes weak nonlinearity, randomness of phases, infinite-box limit, and existence of an inertial interval in wavenumber space (k_0, k_1), where energy input and dissipation are balanced. Under these assumptions, the wave system is energy conserving, and wave kinetic equations describing the wave spectrum have stationary solutions in the form of energy power spectra $k^{-\alpha}$, $\alpha > 0$, [31]. As it was first established in the frame of the model of laminated turbulence, [12], energy spectra have "gaps" formed by exact and quasi-resonances (that is, resonances with small enough resonance broadening). This yields two distinct layers of turbulence in an arbitrary nonlinear wave system – continuous and discrete – and their interplay generates three possible wave turbulent regimes: *kinetic*,[31]; *discrete*, [13], and *mesoscopic*,[32], as it is shown in Fig. 1 (see [6] for more discussion).

From a mathematical point of view, the very special role of resonant solutions has been first demonstrated by Poincaré who proved, using Calogero's

terminology, that a nonlinear ODE is C-integrable if it has no resonance solutions (see [1] and refs. therein). This statement allows the following Hamiltonian formulation [31]:

$$i\,\dot{a}_{\mathbf{k}} \;=\; \partial\mathcal{H}/\partial a^*_{\mathbf{k}}, \tag{1}$$

where $a_{\mathbf{k}}$ is the amplitude of the Fourier mode corresponding to the wavevector $\mathbf{k}$ and the Hamiltonian $\mathcal{H}$ is represented as an expansion in powers $\mathcal{H}_j$ which are proportional to the product of j amplitudes $a_{\mathbf{k}}$. Then the cubic Hamiltonian has the form

$$\mathcal{H}_3 = \sum_{\mathbf{k_1},\mathbf{k_2},\mathbf{k_3}} V^3_{12} a^*_1 a_2 a_3 \delta^1_{23} + \text{ complex conj.},$$

where for brevity we introduced the notation $a_j \equiv a_{\mathbf{k}_j}$ and $\delta^1_{23} \equiv \delta(\mathbf{k_3} - \mathbf{k_1} - \mathbf{k_2})$ is the Kronecker symbol. If $\mathcal{H}_3 \neq 0$, three-wave resonant processes are dominant. These satisfy the resonance conditions:

$$\omega(\mathbf{k}_1) + \omega(\mathbf{k}_2) - \omega(\mathbf{k}_3) = 0 \quad \mathbf{k}_1 + \mathbf{k}_2 - \mathbf{k}_3 = 0, \tag{2}$$

where $\omega(\mathbf{k})$ is a dispersion relation for the linear wave frequency. Further on, the notation ω_k is used for $\omega(\mathbf{k})$. The corresponding dynamical system has a general form

$$i\dot{B}_{\mathbf{k}} = \sum_{\mathbf{k_1},\mathbf{k_2}} \left(V^{\mathbf{k}}_{12} B_1 B_2 \delta^{\mathbf{k}}_{12} + 2 V^{1\,*}_{\mathbf{k}2} B_1 B^*_2 \delta^1_{\mathbf{k}3} \right) \tag{3}$$

(notations B_j are used further on for the resonant modes). If $\mathcal{H}_3 = 0$, four-wave resonances have to be studied, and so on. To confirm that $\mathcal{H}_3 \neq 0$ and three-wave resonances are dominant, one has to find solutions of (2) and check that $V^{\mathbf{3}}_{12} \neq 0$ at least at some resonant triads. Afterwards the corresponding dynamical system has to be studied.

It has been proven in [11] that for a big class of physically relevant dispersion functions ω, the set of all wavevectors satisfying (2) can be divided into non-intersecting classes and solutions of (2) can be looked for in each class separately. This method of q-class decomposition has been developed specially for solving systems of the form (2) in integers; details of its implementation for various rational and irrational dispersion functions are given in [15]. General description of the q-class method and corresponding programming codes are given in [14], in Ch.3 and Appendix correspondingly.

An immediate consequence of the q-class method is that dynamical system (3) can be reduced to *a few dynamical systems* of smaller order, and each of these smaller dynamical systems can be investigated independently

from all others. In [17], construction of a set of reduced dynamical systems corresponding to the solutions of (2) and the systems themselves are given explicitly (as an example, resonances of oceanic planetary waves were considered in the spectral domain $0 \leq m, n \leq 50$). The integrability of some resonance clusters has been studied in [2].

The main goal of the present paper is to study systematically the integrable dynamics of the most frequently met resonance clusters. We begin with a brief introduction of NR-diagrams (NR for nonlinear resonance) which give a handy graphical representation of a generic resonance cluster and allow us to recover uniquely the dynamical system corresponding to each cluster [14].

2 NR-diagrams

In systems with cubic Hamiltonian, a resonant triad is called *primary cluster* (a resonant quartet is a primary cluster in a system with quadric Hamiltonian, and so on). All other clusters (formed by a few primary clusters connected via one of a few joint modes) are called *generic* clusters or simply clusters. The dynamical system for a complex triad in the standard Manley–Rowe form reads

$$\dot{B}_1 = ZB_2^*B_3, \quad \dot{B}_2 = ZB_1^*B_3, \quad \dot{B}_3 = -ZB_1B_2, \tag{4}$$

and is known to be integrable, with two conservation laws in the Manley–Rowe form being

$$I_{23} = |B_2|^2 + |B_3|^2, \; I_{13} = |B_1|^2 + |B_3|^2.$$

Due to the criterion of nonlinear instability for a triad [10], the mode with maximal frequency, ω_3, is unstable while the modes ω_1 and ω_2 are neutral. This means that the form of dynamical systems and accordingly time evolution of the modes belonging to a generic cluster depends crucially on the fact whether joint modes within a cluster are stable or unstable. With the purpose to distinguish between these cases, the notations A-mode (active) and P-mode (passive) are introduced for ω_3-mode and ω_1- and ω_2-modes respectively, [16]. This allows to describe all possible connection types within a generic cluster. For instance, 1-mode connection of two triads can be of AA-, AP- and PP-type; 1-mode connection of three triads can be of AAA-, AAP-, APP-type and PPP-type, 2-mode connection between two triads can be of AA-PP-, AP-AP-, AP-PP- and PP-PP-types, and so on.

In the topological representation [17] of the solution set of (2) this dynamical information has been kept unexplicit, as part of a programming code

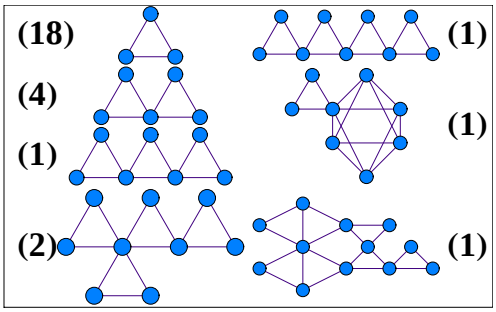

Figure 2: Topological structure of the cluster set for the oceanic planetary waves, $\omega \sim 1/\sqrt{m^2+n^2}$, in the domain $m, n \leq 50$. 7 types of resonance clusters have been found, the number of the clusters of each type is shown in parenthesis. Figure is taken from [17].

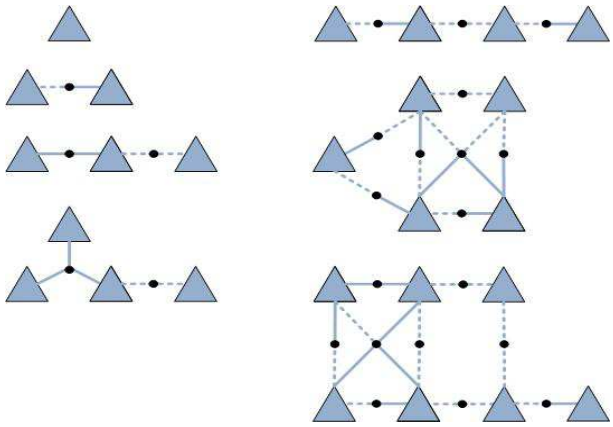

Figure 3: NR-diagrams for some resonance clusters shown in Fig.2.

used to construct dynamical system, while each triad within a cluster was shown as an unmarked triangle (see Fig.2).

More compact graphical representation of a resonance cluster is given by its NR-diagram, [13]. In a NR-diagram each vertex represents not a resonant mode but a *primary cluster*, that is, a triad and a quartet in a three- and four-wave system correspondingly. A NR-diagram in systems with cubic Hamiltonian consists of following building elements – a triangle and two types of half-edges, bold for A-mode and dotted for P-mode. It can be proven ([14], Ch.3) that in this case the form of NR-diagram defines *uniquely* corresponding dynamical system. Examples of NR-diagrams for some resonance clusters shown in Fig.2 are displayed in Fig.3. Below, examples of dynamical

systems are given for two generic clusters shown in Fig.2:

1. Cluster consisting of two triads a and b, whose connecting mode is active in one triad and passive in the other triad, say $B_{3a} = B_{1b}$. In other words, a cluster with one AP-connection. It is called AP-butterfly [16] and its dynamical system is

$$\begin{cases} \dot{B}_{1a} = Z_a B^*_{2a} B_{3a}\,, \quad \dot{B}_{2a} = Z_a B^*_{1a} B_{3a}\,, \quad \dot{B}_{3a} = -Z_a B_{1a} B_{2a} + Z_b B^*_{2b} B_{3b}, \\ \dot{B}_{2b} = Z_b B^*_{3a} B_{3b}\,, \quad \dot{B}_{3b} = -Z_b B_{3a} B_{2b}\,, \end{cases} \tag{5}$$

2. Cluster consisting of three triads a, b and c, with one AA- and one PP-connections, say, $B_{3a} = B_{3b}$ and $B_{1b} = B_{1c}$. The dynamical system reads

$$\begin{cases} \dot{B}_{1a} = Z_a B^*_{2a} B_{3a}, \quad \dot{B}_{2a} = Z_a B^*_{1a} B_{3a}, \quad \dot{B}_{3a} = -Z_a B_{1a} B_{2a} - Z_b B_{1b} B_{2b} \\ \dot{B}_{1b} = Z_b B^*_{2b} B_{3a} + Z B^*_{2c} B_{3c}, \quad \dot{B}_{2b} = Z_b B^*_{1b} B_{3a}, \\ \dot{B}_{2c} = Z_c B^*_{1b} B_{3c}, \quad \dot{B}_{3c} = -Z_c B_{1b} B_{2c}. \end{cases} \tag{6}$$

The Manley–Rowe constants can be written out immediately for each of these systems, being combinations of corresponding constants for each triad. For instance, for (5) they have the form

$$I_{12b} = |B_{1b}|^2 - |B_{2b}|^2, \quad I_{23b} = |B_{2b}|^2 + |B_{3b}|^2, \quad I_{ab} = |B_{1b}|^2 + |B_{3a}|^2 + |B_{3b}|^2. \tag{7}$$

The main difference between NR-diagram and statistical diagrams used in wave turbulence theory and originated from Feynman diagrams can be formulated as follows. Each statistical diagram corresponds to *one term* in the asymptotic expansion and does not allow to compute the amplitudes of the scattering process. On the other hand, a NR-diagram describes *completely* a resonance cluster and allows to write out explicit form of the dynamical system on the modes' amplitudes.

As it will be shown below, connection types within a cluster define indeed the integrability of the corresponding dynamical systems. In order to demonstrate it we will use the notion of dynamical invariant first introduced in [2] which is given in the next section and illustrated by the example of harmonic oscillator.

3 Dynamical invariants

3.1 Definition

From here on, general notations and terminology will follow Olver's book [26] and Einstein convention on repeated indices and $f_{,i} \equiv \partial f / \partial x^i$. Consider

a general N-dimensional system of autonomous evolution equations of the form:

$$\frac{dx^i}{dt}(t) = \Delta^i(x^j(t)), \quad i = 1, \ldots, N. \tag{8}$$

Any scalar function $f(x^i, t)$ that satisfies

$$\frac{d}{dt}\left(f(x^i(t), t)\right) = \frac{\partial}{\partial t} f + \Delta^i f_{,i} = 0$$

is called *a conservation law* in [26]. It is easy to see that this definition gives us two types of conservation laws: (i) those of the form $f(x^i)$ (no explicit time-dependence), and (ii) those of the form $f(x^i, t)$, where the time dependence is explicit. The first type determines an invariant manifold for the dynamical system (8) (*time-independent* conservation law) and the second type constrains the time evolution of the system within the invariant manifold(s) (*time-dependent* conservation law). To keep in mind the difference between these two types of conservation laws, we call the first type just a conservation law (CL), and the second type - a *dynamical invariant*.

We are interested in determining the solution $x^i(t), \quad i = 1, \ldots, N$, of a given dynamical system of the form (8). One possible way to do that is by finding N functionally independent dynamical invariants for the system (8). This is equivalent to finding $(N-1)$ functionally independent conservation laws and *one* dynamical invariant (the equivalence can be proven, for example, using the implicit function theorem).

As it was shown in [3], in some cases the knowledge of only $(N-2)$ functionally independent CLs is enough for constructing explicitly: (i) a new CL functionally independent of the others, and (ii) a corresponding dynamical invariant, determining the solution $x^i(t), \quad i = 1, \ldots, N$. This follows from the Theorem on $(N-2)$–integrability [3], whose formulation is given below for the readers' convenience.

Theorem on $(N-2)$–integrability. *Let us assume that the system (8) possesses a standard Liouville volume density*

$$\rho(x^i) : \ (\rho\Delta^i)_{,i} = 0,$$

and $(N-2)$ functionally independent CLs, $H^1, \ldots, H^{N-2}$. Then a new CL in quadratures can be constructed, which is functionally independent of the original ones, and therefore the system is integrable.

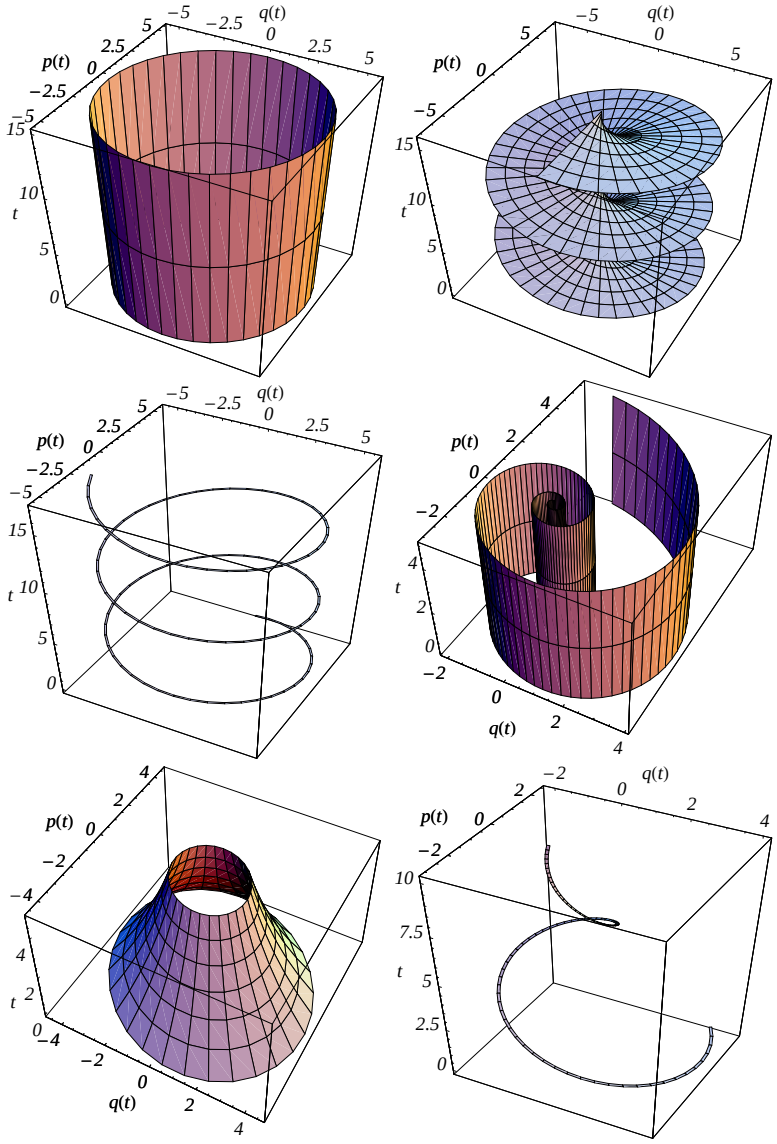

Figure 4: Color online. Upper panel: harmonic oscillator (case $\alpha = 0$): left upper panel, a level surface of conservation law $E(q,p) = 30$, Eq.(10); middle upper panel, a level surface of dynamical invariant $T(q,p,t) = 0$, Eq.(14); right upper panel, solution trajectory $(q(t), p(t))$, Eq.(12), corresponding to $E = 30$, $T = 0$. Lower panel: sub-critically damped harmonic oscillator (case $0 < \alpha < 2$): left lower panel, a level surface of conservation law $C(q,p) = 30$, Eq.(17); middle upper panel, a level surface of dynamical invariant $D(q,p,t) = 20$, Eq.(15); right upper panel, solution trajectory $(q(t), p(t))$, Eq.(18), corresponding to $C = 30$, $D = 20$.

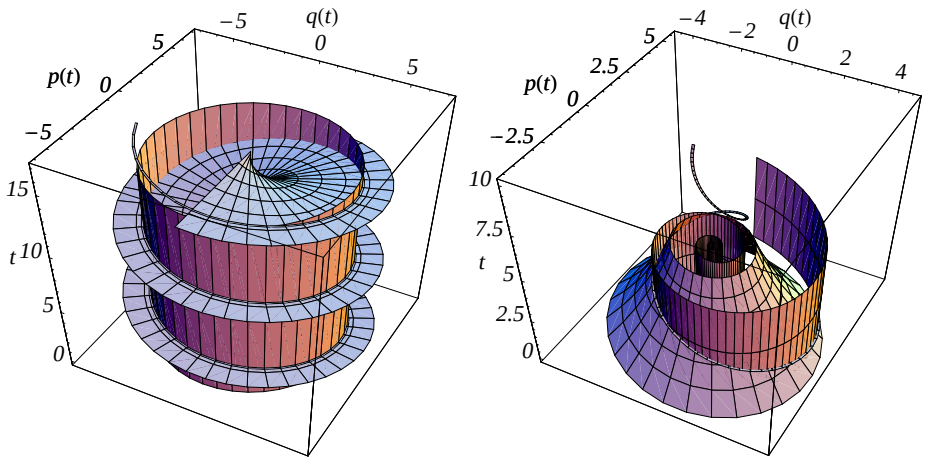

Figure 5: Color online. Left panel: harmonic oscillator (case $\alpha = 0$): combined plot of level surface of conservation law $E(q, p)$, level surface of dynamical invariant $T(q, p, t)$ and solution trajectory $(q(t), p(t))$. Notice the general property that the intersection of the level surfaces of E and T *is* the solution trajectory. Right panel: sub-critically damped harmonic oscillator (case $0 < \alpha < 2$): combined plot of level surface of conservation law $C(q, p)$, level surface of dynamical invariant $D(q, p, t)$ and solution trajectory $(q(t), p(t))$. Notice the general property that the intersection of the level surfaces of C and D *is* the solution trajectory.

3.2 Example: damped harmonic oscillator

3.2.1 Dynamical invariants, CLs and solutions

To illustrate the complementarity of conserved laws and dynamical invariants, we present an illustrative example from mechanics for the case $N = 2$. Consider the damped harmonic oscillator. The equations of motion in non-dimensional form can be written as:

$$\dot{q} = p\,, \quad \dot{p} = -q - \alpha p, \tag{9}$$

where $\alpha \geq 0$ is the damping coefficient. This is a dynamical system of the form (8) with $N = 2$. Now we want to fully determine the solution of the dynamical system (9). For this we need to know both a CL and a dynamical invariant. Indeed, let us consider separately the cases $\alpha = 0$ (harmonic oscillator) and $0 < \alpha < 2$ (sub-critically damped harmonic oscillator).

1. Case $\alpha = 0$. We have the CL

$$E(q,p) = 1/2\left(p^2 + q^2\right) \tag{10}$$

(energy) and the dynamical invariant

$$T(q,p,t) = t - \arctan(q/p). \tag{11}$$

Since

$$\frac{d}{dt}(E(q(t),p(t))) = 0\,, \quad \frac{d}{dt}(T(q(t),p(t),t)) = 0,$$

then we have

$$E(q(t),p(t)) = E_0\,, \quad T(q(t),p(t),t) = T_0,$$

constants depending on the initial conditions $q(0), p(0)$. This information is enough to find the solution $q(t), p(t)$ of the system:

$$q(t) = \sqrt{2E_0}\sin(t - T_0), \quad p(t) = \sqrt{2E_0}\cos(t - T_0) \tag{12}$$

which can be checked by direct substitution in (9).

In Fig.4, upper panel, we show level surface of conservation law $E = 30$ (on the left), level surface of dynamical invariant $T = 0$ (middle) and solution trajectory $q(t), p(t)$ (on the right). This solution is actually the intersection of the level surfaces $E = 30$ and $T = 0$; for completeness of presentation, we show together the level surfaces and the solution in Fig.5 (left panel).

Notice that coordinates q, p are not suitable for a global parametrization of dynamical invariant T, (11), because $\arctan(x)$ is multi-valued. This problem can easily be overcome by using new coordinates (R, θ):

$$q = R\sin\theta\,, \quad p = R\cos\theta \tag{13}$$

which allow us to rewrite T as

$$T(q,p,t) = \tilde{T}(R,\theta,t) = t - \theta, \tag{14}$$

thereby eliminating the ambiguity. The plot of level surface $\tilde{T} = 0$ in the middle upper panel of Fig.4 was done using the parameters (R,t).

2. Case $0 < \alpha < 2$. Let $\alpha/2 = \sin\varphi$, then a dynamical invariant for the system is known:

$$D(q,p,t) = \left(p^2 + q^2 + 2\,p\,q\sin\varphi\right)\exp(2\,t\sin\varphi). \tag{15}$$

We need to find a CL in order to determine the solution. Here we simply state the following CL:

$$C(q,p) = \frac{\cos\varphi}{2}\left(p^2 + q^2 + 2\,p\,q\sin\varphi\right) \times \exp\left[2\tan\varphi\arctan(\frac{q}{p}\sec\varphi + \tan\varphi)\right].$$

The method of construction of this CL is not important right now, it will be detailed in the next section. In Fig.4, lower panel, we show level surface of conservation law $C = 30$ (on the left), level surface of dynamical invariant $D = 20$ (middle) and solution trajectory $q(t), p(t)$ (on the right). This solution corresponds to the intersection of the level surfaces $C = 30$ and $D = 20$; for completeness, the level surfaces and the solution are shown together in Fig.5 (right panel).

Similar to the case of $\alpha = 0$ dynamical invariant, the CL $C(q,p)$ is not globally defined. The following change of variables is needed:

$$q = R\,\sec\varphi\,\sin(\theta - \varphi), \quad p = R\,\cos\theta\,\sec\varphi, \tag{16}$$

in order to parameterize globally the CL. The result is

$$C(q,p) = \tilde{C}(R,\theta) = \frac{\cos\varphi}{2}R^2\exp(2\theta\tan\varphi). \tag{17}$$

It is important to realize that the two changes of variables (13) and (16) are suggested by the form of the respective invariants. Moreover, in the new variables (R,θ), both T and C take a simpler form (see (14),(17)). The reason for it is clear in the case $\alpha = 0$ because (R,θ) are the well-known action-angle variables. In the general case, the variables (R,θ) determine a covering of the original variables.

The solution of the dynamical system is finally

$$q(t) = \frac{\sqrt{D}\,\sin(t\,\cos\varphi + \frac{1}{2}\log(\frac{C}{D})\cot\varphi - \varphi)}{\cos\varphi\,\exp(t\,\sin\varphi)} \tag{18}$$

$$p(t) = \frac{\sqrt{D}\,\cos(t\,\cos\varphi + \frac{1}{2}\log(\frac{C}{D})\cot\varphi)}{\cos\varphi\,\exp(t\,\sin\varphi)}. \tag{19}$$

3.2.2 Description of a laboratory experiment

To check the constancy of the conservation law $C(q,p)$ in a school laboratory experiment, we give here detailed description of the possible experiment in the case of sub-critical damping $0 < \alpha < 2$. Moreover, we provide evidence of the practical and physical interest of the conservation law $C(q,p)$: it can be used to measure the damping coefficient α. A simple pendulum oscillating at small amplitudes is easy to construct, consisting of a massive bob attached to the ceiling by a light (i.e. massless) string or rod. Damping can be easily introduced by attaching to the pendulum rod a sheet made of a light material. For small amplitudes, the angular frequency of the oscillations is given by $\omega = \sqrt{g/L}$, where $g \approx 9.8[m/s^2]$ is the acceleration of gravity and L is the pendulum length. We assume ω to be known, though of course it could be measured experimentally. From now on, we choose units where $\omega = 1$, so the damped pendulum equations for small amplitudes reduces to the system (9), where q is the position of the oscillating bob and p is its velocity.

With the aid of cheap electronic detection equipment it is possible to measure accurately the time t, position q and velocity p of the oscillating bob at certain instances, namely when the bob passes near a detector. This data is sent to a computer database and analyzed with a software that comes along with the detection equipment. As a result one obtains a set of data points of the form

$$(q_n, p_n, t_n)\,, \quad n = 0, \ldots, N \tag{20}$$

With the aid of only one detector, we can in principle measure data at instances when $q_n = 0$. To wit, we first calibrate the detector by setting the $q = 0$ coordinate as the equilibrium position of the mass. An experimental realization consists in producing a small amplitude oscillation and acquiring data points of the form (20). By looking at (16), these instances correspond to

$$\theta_n = \varphi + n\pi, \quad p_n = (-1)^n R_n,$$

where φ is the unknown parameter related to the damping coefficient by $\alpha = 2\sin\varphi$. From (17) we obtain data values

$$C_n = \frac{\cos\varphi}{2} p_n^2 \exp(2(\varphi + n\pi)\tan\varphi).$$

If C is a conservation law, then C_n must be constant, independent of n. Therefore we should have

$$p_n^2 \exp(2n\pi\tan\varphi) = \text{const} = p_0^2.$$

In practice one can measure $\tan\varphi$ by finding a linear fit of $\log|p_n|$ versus n:

$$\log|p_n| = \log|p_0| - n\pi\tan\varphi\,, \quad n = 1, \ldots, N. \tag{21}$$

Once $\tan\varphi$ has been obtained, the damping coefficient α is readily computed.

Notice that one could use alternatively the dynamical invariant $D(q,p,t)$ to compute α, from the data (20). Setting $t_0 = 0$, from (15) we obtain

$$D_n = p_n^2 \exp(2t_n \sin\varphi) = \text{const} = p_0^2.$$

We can measure $\sin\varphi$ by finding a linear fit of $\log|p_n|$ versus t_n:

$$\log|p_n| = \log|p_0| - t_n \sin\varphi\,, \quad n = 1,\ldots,N. \tag{22}$$

Finally, notice that these two ways to measure the damping coefficient imply a third way: by comparing (21) and (22) we solve for the data times

$$t_n = n\pi/\cos\varphi\,, \quad n = 1,\ldots,N.$$

In this case, a simple linear fit of t_n as a function of n will allow us to obtain φ and thereby the damping coefficient α.

3.2.3 Construction of conservation law

To illustrate the procedure of construction of a conservation law, we take as an example the sub-critically damped harmonic oscillator, i.e. (9) with $0 < \alpha < 2$. Here $N = 2$ and $\Delta^1 = p, \quad \Delta^2 = -q - \alpha p$. The dynamical system is just 2-dimensional and we will write it as a vector $(\Delta^1, \Delta^2)^T$. The Theorem requires the existence of a standard Liouville volume density $\rho(x^1, x^2)$ satisfying

$$(\rho\Delta^1)_{,1} + (\rho\Delta^2)_{,2} = 0, \tag{23}$$

and does not require the knowledge of conservation laws. In general, a Liouville density, solution of (23), is interpreted as follows. A small region $\mathcal{R}(t)$ with a volume $V(t)$ in phase space (x_1, x_2), will evolve in time due to the dynamical system (9). Then, ρ is defined in such a way that the product $\rho\, V(t)$ is conserved in time as $\mathcal{R}(t)$ evolves. For the harmonic oscillator, it is well known that the volume of $\mathcal{R}(t)$ is preserved, i.e., a constant function is a Liouville density. For the damped harmonic oscillator, a direct check shows that a Liouville density is $\rho(q,p) = \left(q^2 + p^2 + 2\alpha\, q\, p\right)^{-1}$. With this information we just need to solve (24) for H:

$$\begin{pmatrix} 0 & 1 \\ -1 & 0 \end{pmatrix} \begin{pmatrix} H_{,1} \\ H_{,2} \end{pmatrix} = \begin{pmatrix} \rho\,\Delta^1 \\ \rho\,\Delta^2 \end{pmatrix}. \tag{24}$$

The answer can be obtained by direct integration (see [2] for more details):

$$H(q,p) = -\left(\frac{q\,\alpha\, \arctan\left(\frac{2\,p + q\,\alpha}{\sqrt{-\left(q^2\,(-4+\alpha^2)\right)}}\right)}{\sqrt{-\left(q^2\,(-4+\alpha^2)\right)}} \right) + \frac{\log(p^2 + q^2 + p\,q\,\alpha)}{2} \tag{25}$$

The conservation law $C(q,p)$ given by Eq.(16) is a function of H, chosen for its nice form:

$$C = \frac{\cos\varphi}{2}\exp(2H).$$

4 Triad

As it was shown above, the notion of dynamical invariant is an important tool for constructing new physically relevant conservation laws that can afterwards be studied in a simple laboratory experiment. In this section we would like to use this approach to prove integrability of a complex triad with dynamical system (4). Though integrability of (4) is a well-known fact, the explicit solution of (4) is usually written for a particular case, namely, when the dynamical phase – a phase combination corresponding to the chosen resonance conditions – is either zero or constant ([24], p.132, Eq.(6.7); [27], p.156, Eq.(3.26.19), etc.).

On the other hand, it is well known that dynamical phases play a substantial role in the dynamics of resonant clusters, e.g. [29], and their effect can easily be observed in numerical simulations, [3]. This was our motivation for constructing first an explicit solution in the amplitude-phase presentation, for (26). Another important point is that an elastic pendulum with suitably chosen parameters can be used as a mechanical model of a resonant triad, and the results can be applied for the description of large-scale motions in the Earth's atmosphere, e.g. [20], In fact, this simple mechanical model can be used for a laboratory study of dynamical characteristics of primary clusters in an *arbitrary* system with cubic Hamiltonian.

4.1 Integrability

In this case the system can be reduced to $N = 4$ (see [2] for more details), the Theorem on $(N-2)$–integrability can be applied and we obtain the following CL:

$$H_T = \mathrm{Im}(B_1 B_2 B_3^*)\,,$$

which is the canonical Hamiltonian for this case and can, of course, be written out directly. A dynamical invariant for this system was originally presented in [2], in terms of the three real roots $R_1 < R_2 < R_3$ of the cubic polynomial

$$x^3+x^2 = 2/27-(27H_T^2-(I_{13}+I_{23})(I_{13}-2I_{23})(I_{23}-2I_{13}))/27(I_{13}^2-I_{13}I_{23}+I_{23}^2)^{3/2}\,,$$

but these roots' dependence on the coordinates or the CLs was not made explicit. Moreover, the explicit solution for the amplitudes C_j and phases θ_j

in the amplitude-phase representation $B_j = C_j \exp(i\theta_j)$ was not provided. Here we improve the form of dynamical invariant and also produce explicit and useful expressions for the full solution, based on the trigonometric representation of the three real roots in the so-called *Casus Irreducibilis*.

4.2 Amplitude-phase representation

Sys.(4) in the standard amplitude-phase representation $B_j = C_j \exp(i\theta_j)$ reads:

$$\begin{cases} \dot{C}_1 = ZC_2C_3\cos\varphi, \quad \dot{C}_2 = ZC_1C_3\cos\varphi, \\ \dot{C}_3 = -ZC_1C_2\cos\varphi, \quad \dot{\varphi} = -Z\,H_T(C_1^{-2} + C_2^{-2} - C_3^{-2}). \end{cases} \tag{26}$$

where $\varphi = \theta_1 + \theta_2 - \theta_3$ is the dynamical phase. The conservation laws (5) do not change their form in the new variables: $I_{23} = C_2^2 + C_3^2$, $I_{13} = C_1^2 + C_3^2$, but the Hamiltonian H_T reads now $H_T = C_1C_2C_3\sin\varphi$. Let us introduce new variables:

$$\rho = I_{23}/I_{13} \tag{27}$$

and $\alpha \in [0, \pi]$ defined by

$$\cos\alpha = \frac{(-2 + 3\,\rho + 3\,\rho^2 - 2\,\rho^3)\;{I_{13}}^3 - 27\,{H_T}^2}{2\,(1 - \rho + \rho^2)^{\frac{3}{2}}\,{I_{13}}^3}\,. \tag{28}$$

Notice that $|\cos\alpha| \leq 1$ for dynamically accessible system's configurations. Indeed, the use of intermediate variables $p = 2\,(1 - \rho + \rho^2)^{\frac{3}{2}}$ and $q = -2 + 3\,\rho + 3\,\rho^2 - 2\,\rho^3$, allows one to conclude immediately that $p \geq 0$ and $p \geq |q| \quad \forall\,\rho$. Both inequalities become equalities if $\rho = 0$ or $\rho = 1$. This yields

$$\left(H_T^2\right)_{\max} = \left(\frac{I_{13}}{3}\right)^3 (p + q) \geq 0\,, \quad \text{for} \quad \cos\alpha = -1,$$

and $(\cos\alpha)_{\max} = q/p \leq 1\,, \quad \text{for} \quad H_T = 0$, where $(H_T^2)_{\max}$ and $(\cos\alpha)_{\max}$ are maximum values of H_T^2 and $\cos\alpha$ correspondingly.

Now, the solution of (26) is obtained in terms of Jacobian functions with modulus

$$\mu = \cos\left(\frac{\alpha}{3} + \frac{\pi}{6}\right) / \cos\left(\frac{\alpha}{3} - \frac{\pi}{6}\right)\,, \tag{29}$$

and period

$$T = \frac{\sqrt{2}\,3^{\frac{1}{4}}\,K\,(\mu)}{Z\,(1 - \rho + \rho^2)^{\frac{1}{4}}\,\sqrt{\cos(\frac{\alpha}{3} - \frac{\pi}{6})}\,\sqrt{I_{13}}}\,, \tag{30}$$

where $K(\mu)$ is the complete elliptic integral of the first kind.

4.3 Solutions for amplitudes

We present explicit expressions for the amplitude squares. The convention used here is that the amplitudes are positive, which is the generic situation when $H_T \neq 0$. In this convention, when $H_T = 0$ the individual phases have discontinuities in time to account for the amplitudes' sign changes. The amplitude squares are proportional to the modes' energies and can be of great use for physical applications:

$$\begin{cases} C_1^2(t) = -\mu \left(\frac{2K(\mu)}{Z\,T}\right)^2 \mathbf{sn}^2\left(2\,K(\mu)\,\frac{(t-t_0)}{T}, \mu\right) \\ +\frac{I_{13}}{3}\left(2-\rho+2\,\sqrt{1-\rho+\rho^2}\,\cos\left(\frac{\alpha}{3}\right)\right), \\ C_2^2(t) = -\mu \left(\frac{2K(\mu)}{Z\,T}\right)^2 \mathbf{sn}^2\left(2\,K(\mu)\,\frac{(t-t_0)}{T}, \mu\right) \\ +\frac{I_{13}}{3}\left(2\rho-1+2\,\sqrt{1-\rho+\rho^2}\,\cos\left(\frac{\alpha}{3}\right)\right), \\ C_3^2(t) = \mu \left(\frac{2K(\mu)}{Z\,T}\right)^2 \mathbf{sn}^2\left(2\,K(\mu)\,\frac{(t-t_0)}{T}, \mu\right) \\ +\frac{I_{13}}{3}\left(\rho+1-2\,\sqrt{1-\rho+\rho^2}\,\cos\left(\frac{\alpha}{3}\right)\right), \end{cases} \tag{31}$$

where $\mathbf{sn}(\cdot,\mu)$ is Jacobian elliptic function and t_0 is given in terms of the initial conditions for the amplitudes $C_1^2(0), C_2^2(0), C_3^2(0)$ and t_0 is defined by the initial conditions as:

$$t_0 = \text{sign}(\cos\varphi(0))\,\frac{T}{2\,K(\mu)} \times F\left(\arcsin\sqrt{x_0}, \mu\right), \tag{32}$$

where

$$x_0 = \frac{\cos\left(\frac{\alpha}{3}\right)}{\sqrt{3}\,\cos\left(\frac{\alpha}{3}+\frac{\pi}{6}\right)} + \frac{Z^2\,T^2\,(C_3^2(0) - C_2^2(0) - C_1^2(0))}{12\,\mu\,K(\mu)^2} \tag{33}$$

and $F(\cdot,\mu)$ is the elliptic integral of the first kind.

Notice that each equation in (31) is a sum of two terms where the left terms are time-dependent and the right terms are not. Each right term, for instance

$$\frac{I_{13}}{3}\left(2-\rho+2\,\sqrt{1-\rho+\rho^2}\,\cos\left(\frac{\alpha}{3}\right)\right)$$

can be written explicitly as a function of conserved quantities I_{13}, I_{23}, H_T (expressions for ρ and α are given by (27),(28)) and is, therefore, defined by the initial conditions.

The same is true for μ and T as it follows from (29) and (30). In particular, one can use the equations in (31) to determine the minimum and maximum accessible values of each amplitude (using the fact that $\mathbf{sn}^2$ oscillates between 0 and 1). The characteristic energy variation of any resonant mode E_{mode}, between these minimum and maximum values, has a very simple form: $E_{mode}(t) \sim \mathbf{sn}^2(k\,t, \mu)$.

4.4 Solution for dynamical phase

The dynamical phase satisfies an evolution equation:

$$\dot{\varphi} = -Z\, H_T(C_1^{-2} + C_2^{-2} - C_3^{-2}). \tag{34}$$

The solution for the dynamical phase **cannot** be obtained by simply replacing the solution for the amplitudes in the Hamiltonian $H_T = C_1 C_2 C_3 \sin\varphi$ and solving for φ. The reason is that non-zero φ generically evolves between 0 and π, crossing the value $\varphi = \pi/2$ periodically. This implies that $\sin^{-1}$ is double-valued and thus it is not possible to obtain φ in a unique way.

Another way to obtain the solution for dynamical phase might be integrating (34) in time, using the solution for the amplitude squares, (31), but this way is also rather involved. On the other hand, some simple considerations allow us to find an analytical expression for the dynamical phase. Indeed, let us rewrite (26), taking into account that $\frac{d}{dt}C_1^2 = 2C_1\dot{C}_1$ and $H_T = C_1 C_2 C_3 \sin\varphi$:

$$\frac{d}{dt}C_1^2 = 2ZC_1C_2C_3\cos\varphi = 2Z H_T \cot\varphi\,.$$

This equation can be solved for φ in each of the disjoint domains $(0,\pi)$ and $(-\pi,0)$:

$$\varphi(t) = \mathrm{sign}(\varphi(0))\,\mathbf{arccot}\left(\frac{\mathrm{sign}(\varphi(0))\,\frac{d}{dt}C_1^2}{2\,Z\,H_T}\right),$$

using the convention that the function **arccot** takes values on $(0,\pi)$. Using solution (31) together with the identity $\mathbf{sn}'(x,\mu) = \mathbf{cn}(x,\mu)\mathbf{dn}(x,\mu)$ we arrive at an explicit expression for the dynamical phase:

$$\varphi(t) = \mathrm{sign}(\varphi_0)\,\mathbf{arccot}\left(-\frac{\mu}{|H_T|}\left(\frac{2K(\mu)}{Z\,T}\right)^3 y\right), \tag{35}$$

$$y = \mathbf{sn}\,\mathbf{cn}\,\mathbf{dn}\left(2\,K(\mu)\,\frac{(t-t_0)}{T},\mu\right) \tag{36}$$

where $\mathbf{sn}\,\mathbf{cn}\,\mathbf{dn}(\cdot,\mu) \equiv \mathbf{sn}(\cdot,\mu)\,\mathbf{cn}(\cdot,\mu)\,\mathbf{dn}(\cdot,\mu)$.

The restriction to the domain $\varphi \in (-\pi,0)\cup(0,\pi)$ is quite general: if φ is initially in the domain $(n\,\pi,(n+1)\,\pi)\,, n \in \mathbb{Z}$, one can take φ to either $(-\pi,0)$ or $(0,\pi)$ by an appropriate shift of $2\,m\,\pi\,, m \in \mathbb{Z}$, without changing the evolution equations. Due to its special dynamics, the phase will remain in the domain where it was initially.

4.5 Dynamical invariant

Below we present a dynamical invariant for (26) which has been used for the constructing the solution (31). Recall that a dynamical invariant depends on time, amplitudes and phases: $S(t, C_1, C_2, C_3, \varphi)$, with the property that it is a constant along any solution of the dynamical system. Generically, only local expressions can be obtained for a dynamical invariant, due to the multi-valuedness of the inverse functions involved. In this particular case, however, since we know the period of any trajectory, this multi-valuedness can be eliminated partially by patching appropriately local expressions yielding

$$S(t, C_1, C_2, C_3, \varphi) = t - \left\lfloor \frac{2(t-t_0)+T}{2\,T} \right\rfloor T + \frac{(-1)^{\left\lfloor \frac{2(t-t_0)+T}{T} \right\rfloor} T}{2\,K(\mu)} F\left(\arcsin\sqrt{x_t}, \mu\right) , \tag{37}$$

where $\lfloor \cdot \rfloor$ is the floor function and x_t can be obtained from the expression (33) for x_0 by substituting $C_j(t)$ instead of $C_j(0)$, for all $j = 1, 2, 3$.

This dynamical invariant satisfies $S(t, C_1(t), C_2(t), C_3(t), \varphi(t)) = t_0 \quad \forall t$, where t_0 is given in equation (32), and is an improvement of the corresponding formula presented in [2].

In Fig. 6, upper panel, we show, for fixed $I_{13} = 2.00$ and $I_{23} = 2.06$: isosurface of conservation law $H_T = 0.763$, isosurface of dynamical invariant $S = 2.69$, solution trajectory and combined plot, in the domain (C_1, φ, t).

In the middle of the upper panel, the surface $S = 2.69$ is a helicoidal surface revolving around a vertical axis. This axis is the surface's natural interior boundary: the constant-in-time trajectory corresponding to the highest possible value of $|H_T|$ for given I_{13}, I_{23} (obtained from the condition $\cos\alpha = -1$). In the present case, the highest possible value of $|H_T|$ is 1.114. This trajectory is physically interpreted as 'maximum interference', due to the fact that the modes do not interact. The dynamical phase is constant: $\varphi(t) = \pi/2 \,\forall\, t$, and all amplitudes are constant as well: from the condition $\mu = 0$ and equations (31), we obtain in this case: $C_1^2(t) = 1.33$, $\forall\, t$. The exterior boundary of the surface is the piecewise continuous trajectory corresponding to the limit $H_T = 0$: in this limit the surface becomes non-differentiable at the 'corners' $C_1^2 = 0, I_{13}$, $\varphi = 0, \pi$, due to the fact that the dynamical phase φ is only piecewise continuous for $H_T = 0$. This trajectory corresponds to the usual case treated in textbooks, when amplitudes are considered real and individual phases vanish.

By looking at this figure we notice that the period T decreases with increasing H_T: the trajectories closer to the exterior boundary are more

elongated than the trajectories closer to the interior boundary. In fact, from formula (30) one can prove this property analytically. In Fig. 7 we plot the period T as a function of H_T. We observe in this case a reduction of the period by a factor 0.5 when H_T is changed from 0 to $H_{\max} = 1.114$.

In Fig. 6, lower panel, on the left and in the middle, combined plots are shown to clarify that the solution trajectory is the intersection of the isosurfaces of Hamiltonian and dynamical invariant. On the right, we show a combined plot of level surfaces of Manley–Rowe conservation laws I_{13}, I_{23} in the domain (C_1^2, C_2^2, C_3^2).

4.6 Special case $H_T = 0$

Direct substitution shows that if we put $H_T = 0$, then new modulus and period take the form

$$\mu = \rho \quad \text{and} \quad T = \frac{2K(\rho)}{Z\sqrt{I_{13}}}$$

correspondingly, while the solutions for the amplitude squares read

$$\begin{cases} \tilde{C}_1^2(t) = \mathrm{dn}^2((t-t_0)\ Z\sqrt{I_{13}}, \rho)\, I_{13} \\ \tilde{C}_2^2(t) = \mathrm{cn}^2((t-t_0)\ Z\sqrt{I_{13}}, \rho)\, I_{23} \\ \tilde{C}_3^2(t) = \mathrm{sn}^2((t-t_0)\ Z\sqrt{I_{13}}, \rho)\, I_{23}\,. \end{cases} \tag{38}$$

As for the dynamical phase, from Eq.(35) it is seen that in the limit $H_T \to 0$ it behaves as a step function, jumping from 0 to $\pi\,\mathrm{sign}(\varphi(0))$:

$$\widetilde{\varphi}(t) = \frac{\pi\,\mathrm{sign}(\varphi(0))}{2}\left(1 - (-1)^{\left\lfloor \frac{2(t-t_0)}{T} \right\rfloor}\right).$$

To understand the meaning of this behaviour, notice that the Hamiltonian H_T is vanishing for $\varphi = n\,\pi$, $n \in \mathbb{Z}$. The abrupt jumps of the dynamical phase is due to the jumps of the individual phases (solution not shown). These jumps replace the changes of sign of the modes' amplitudes in the usual textbook descriptions.

As it was shown in [3], initial dynamical phase not in $\mathbb{Z}\,\pi$ substantially affects the magnitudes of resonantly interacting modes during the evolution, not only in a triad but also in a butterfly. This fact might have important implications (see [3], Discussion), for instance, for interpreting results of numerical simulations and for performing laboratory experiments.

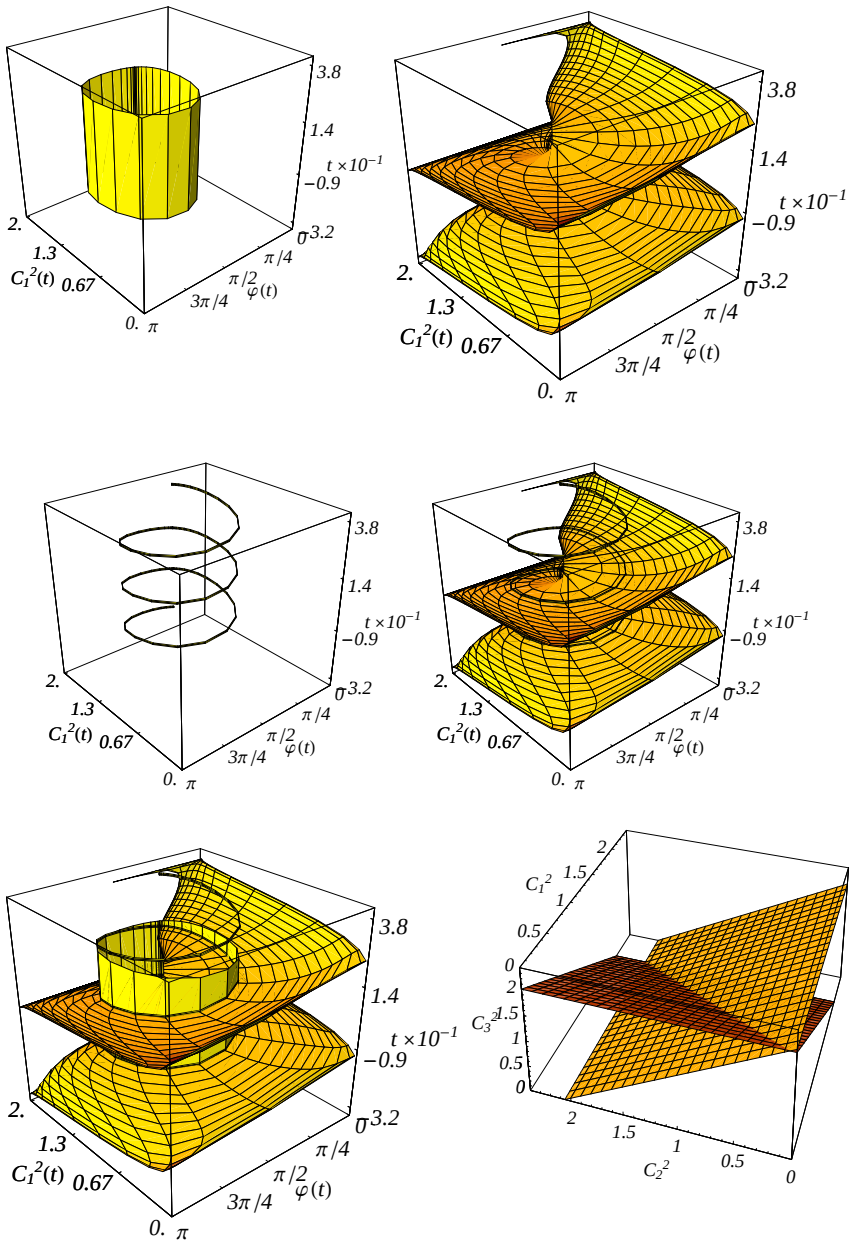

Figure 6: Color online. **Upper panel:** Triad system in coordinates (C_1^2, φ, t), with fixed values of the Manley-Rowe conservation laws: $I_{13} = 2.00$ and $I_{23} = 2.06$. **Left:** level surface of conservation law $H_T = 0.763$. **Middle:** level surface of dynamical invariant $S = 2.69$, Eq.(37). **Right:** solution trajectory $(C_1^2(t), \varphi(t))$, Eqs.(31),(35), corresponding to $H_T = 0.763, S = 2.69$. **Lower panel: Left:** combined plot of level surface of dynamical invariant $S = 2.69$ and solution trajectory $(C_1(t)^2, \varphi(t))$. **Middle:** combined plot of level surface of conservation law $H_T = 0.763$, level surface of dynamical invariant $S = 2.69$ and solution trajectory $(C_1^2(t), \varphi(t))$. Notice the general property that the intersection of the level surfaces of H_T and S *is* the solution trajectory. **Right:** combined plot of Manley-Rowe conservation laws $I_{13} = 2.00$ and $I_{23} = 2.06$, in coordinates (C_1^2, C_2^2, C_3^2) .

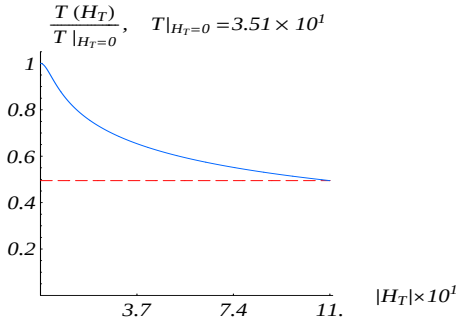

Figure 7: Color online. With fixed values of the Manley-Rowe conservation laws: $I_{13} = 2.00$ and $I_{23} = 2.06$, plot of period T from Eq.(30) as a function of H_T, normalized with respect to the period at $H_T = 0$. The decreasing character is a generic feature of this function.

5 Generic clusters

In a three-wave resonance systems the most frequently met clusters are isolated triads or clusters consisting of two variously connected triads, e.g.[11, 15, 16, 18]. Below we show how to construct new CLs making use of the notion of dynamical invariant. In the last subsection, another method is briefly outlined which was presented in [30] and allows one to prove, in some cases, integrability of bigger clusters.

5.1 Butterfly

A *PP-butterfly* consists of two triads a and b, with wave amplitudes B_{ja}, B_{jb}, $j = 1, 2, 3$, and connecting mode, say $B_{1a} = B_{1b} = B_1$, is passive in both triads. The dynamical system for PP-butterfly reads

$$\begin{cases} \dot{B}_1 = Z_a B^*_{2a} B_{3a} + Z_b B^*_{2b} B_{3b} \,, \quad \dot{B}_{2a} = Z_a B^*_1 B_{3a} \,, \\ \dot{B}_{2b} = Z_b B^*_1 B_{3b} \,, \quad \dot{B}_{3a} = -Z_a B_1 B_{2a} \,, \quad \dot{B}_{3b} = -Z_b B_1 B_{2b} \,. \end{cases} \tag{39}$$

Figure 8: NR-diagram for PP-butterfly.

We have studied this in [2]; we present here the results in order to compare the dynamics of different butterfly types and confirm the qualitative analysis given in [16]. Sys.(39) has 3 quadratic CLs analogous to (5) and 1 cubic CL corresponding to its Hamiltonian:

$$\begin{cases} I_{23a} = |B_{2a}|^2 + |B_{3a}|^2\,, \quad I_{23b} = |B_{2b}|^2 + |B_{3b}|^2\,, \\ I_{ab} = |B_1|^2 + |B_{3a}|^2 + |B_{3b}|^2\,, \\ H_{PP} = \mathrm{Im}(Z_a B_1 B_{2a} B_{3a}^* + Z_b B_1 B_{2b} B_{3b}^*). \end{cases} \tag{40}$$

Standard amplitude–phase representation. Here, one can rewrite the cubic conservation law as

$$H_{PP} = C_{PP}\left(Z_a C_{2a} C_{3a} \sin\varphi_a + Z_b C_{2b} C_{3b} \sin\varphi_b\right). \tag{41}$$

Here

$$\varphi_a = \theta_{1a} + \theta_{2a} - \theta_{3a}, \quad \varphi_b = \theta_{1b} + \theta_{2b} - \theta_{3b}$$

are dynamical phases and $C_{(PP)}$ is the real amplitude of a common mode in PP-butterfly. This allows us to reduce Sys.(39) to only four real equations:

$$\begin{cases} \dot{C}_{3a} = -Z_a C_{PP} C_{2a} \cos\varphi_a\,, \quad \dot{C}_{3b} = -Z_b\, C_{PP} C_{2b} \cos\varphi_b\,, \\ \dot{\varphi}_a = -H_{PP}(C_{PP}^{-2} + C_{2a}^{-2} - C_{3a}^{-2}), \quad \dot{\varphi}_b = -H_{PP}(C_{PP}^{-2} + C_{2b}^{-2} - C_{3b}^{-2}). \end{cases} \tag{42}$$

Now the overall dynamics of the PP-butterfly is confined to a 3-dimensional manifold. The same can be done for the two other types of butterflies.

Modified amplitude-phase representation. The following change of variables was suggested in [2]:

$$\alpha_a = \arctan\left(C_{3a}/C_{2a}\right), \quad \alpha_b = \arctan\left(C_{3b}/C_{2b}\right)\,.$$

with the inverse transformation being

$$\begin{cases} C_{2a} = \sqrt{I_{23a}}\cos\alpha_a\,, \quad C_{3a} = \sqrt{I_{23a}}\sin\alpha_a\,, \\ C_{2b} = \sqrt{I_{23b}}\cos\alpha_b\,, \quad C_{3b} = \sqrt{I_{23b}}\sin\alpha_b\,, \end{cases} \tag{43}$$

This change of variables allows further substantial simplification of (39) and (42):

$$\begin{cases} \dot{\alpha}_a = -Z_a C_{PP}\cos\varphi_a, \quad \dot{\alpha}_b = -Z_b C_{PP}\cos\varphi_b\,, \\ \dot{\varphi}_a = Z_a C_{PP}\left(\cot\alpha_a - \tan\alpha_a\right)\sin\varphi_a - H_{PP}/C_{PP}^2, \\ \dot{\varphi}_b = Z_b C_{PP}\left(\cot\alpha_b - \tan\alpha_b\right)\sin\varphi_b - H_{PP}/C_{PP}^2. \end{cases} \tag{44}$$

In these new variables, the amplitude $C_{PP} > 0$ reads

$$C_{PP} = \sqrt{I_{ab} - I_{23a}\sin^2\alpha_a - I_{23b}\sin^2\alpha_b} \tag{45}$$

and the Hamiltonian is now

$$H_{PP} = \frac{C_{PP}}{2} Z_a I_{23a} \sin\varphi_a \sin 2\alpha_a + \frac{C_{PP}}{2} Z_b I_{23b} \sin\varphi_b \sin 2\alpha_b. \tag{46}$$

Eqs. (44)–(46) represent the final form of our three-dimensional general system in the modified amplitude-phase presentation.

Of course, the form of the conservation laws is arbitrary in the sense that any set of functionally independent CLs will be suitable. For instance, in the case $H_{PP} = 0$ we could choose the conserved quantity

$$A_b = \sin\varphi_b \sin 2\alpha_b \quad \text{instead of} \quad A_a = \sin\varphi_a \sin 2\alpha_a$$

but not both because they are functionally dependent:

$$Z_a I_{23a} A_a + Z_b I_{23b} A_b \equiv 0.$$

Generally, we try to find the simplest presentation for our new constants of motion.

Analogously with the previous case, *AA-butterfly* is a two-triad cluster with a common mode which is A-mode in both triads, $B_{3a} = B_{3b}$. Dynamical system and Manley–Rowe constants read:

$$\begin{cases} \dot{B}_{1a} = Z_a B^*_{2a} B_{3a}\,, \;\; \dot{B}_{1b} = -Z_b B^*_{2b} B_{3a}\,, \;\; \dot{B}_{2a} = Z_a B^*_{1a} B_{3a}\,, \\ \dot{B}_{2b} = Z_b B^*_{1b} B_{3a}\,, \;\; \dot{B}_{3a} = -Z_a B_{1a} B_{2a} - Z_b B_{1b} B_{2b}\,. \end{cases} \tag{47}$$

$$I_{12a} = |B_{1a}|^2 - |B_{2a}|^2\,, \;\; I_{12b} = |B_{1b}|^2 - |B_{2b}|^2\,, \;\; I_{ab} = |B_{1a}|^2 + |B_{3a}|^2 + |B_{3b}|^2\,. \tag{48}$$

The integrability of (47) can be investigated along the same lines as for (39)

Figure 9: NR-diagram for AA-butterfly.

above. The analysis is omitted here. We just partly outline one particular case of this cluster: *AA*-ray, which can be regarded as a degenerate *AA*-butterfly, so that $\omega_{1b} = \omega_{2b} = \omega_3/2$. In this case, the dynamical system obtained from first principles will have the form

$$\dot{B}_{1a} = Z_a B^*_{2a} B_3\,, \;\; \dot{B}_b = Z_b B^*_b B_3\,, \;\; \dot{B}_{2a} = Z_a B^*_{1a} B_3\,, \;\; \dot{B}_3 = -Z_a B_{1a} B_{2a} - 2 Z_b B_b^2\,. \tag{49}$$

Notice that there is a factor 2 in the last term of last equation, which would not appear if we made the direct substitution $B_{1b} = B_{2b} = B_b$ into system (47). Rather, the simple change of variables $B_{1b} = B_{2b} = \sqrt{2}B_b$ will transform the AA-butterfly (47) into the ray equations (49). This means in particular that integrable cases of AA-butterfly can be directly mapped to some integrable cases of AA-ray. Another interesting point is that AA-ray cluster might also have a nice mechanical model - Wilberforce pendulum (P. Lynch, private communication, 2009).

Conservation laws for AA-ray are inherited from conservation laws for AA-butterfly:

$$I_{12a} = |B_{1a}|^2 - |B_{2a}|^2\,, \quad I_{ab} = |B_{1a}|^2 + 2|B_b|^2 + |B_3|^2\ , \tag{50}$$

$$H_{\rm ray} = \mathrm{Im}(-Z_a B_{1a} B_{2a} B_3^* - 2Z_b B_b^2 B_3^*), \tag{51}$$

with dynamical phases

$$\varphi_a = \theta_{1a} + \theta_{2a} - \theta_3, \quad \varphi_b = 2\theta_b - \theta_3.$$

This reduces four complex equations (49) to only four real ones:

$$\begin{cases} \dot{C}_{1a} = Z_a C_{2a} C_3 \cos\varphi_a\,, \quad \dot{C}_b = Z_b C_b C_3 \cos\varphi_b\,, \\ \dot{\varphi}_a = -Z_a C_3 \left(\frac{C_{2a}}{C_{1a}} + \frac{C_{1a}}{C_{2a}}\right) \sin\varphi_a + H_{\rm ray}/C_3^2, \\ \dot{\varphi}_b = -2Z_b C_3 \sin\varphi_b + H_{\rm ray}/C_3^2\,, \end{cases} \tag{52}$$

with Hamiltonian

$$H_{\rm ray} = -C_3\left(Z_a C_{1a} C_{2a} \sin\varphi_a + 2Z_b C_b^2 \sin\varphi_b\right) \tag{53}$$

in terms of the amplitudes and phases.

Consider the simple case when initially $\varphi_a = \varphi_b = 0$. Then $H_{\rm ray} = 0$, phases remain zero for all times, and the equations of motion reduce to

$$\dot{C}_{1a} = Z_a C_{2a} C_3\,,\ \dot{C}_{2a} = Z_a C_{1a} C_3\,,\ \dot{C}_b = Z_b C_b C_3\,,\ \dot{C}_3 = -Z_a C_{1a} C_{2a} - 2Z_b C_b^2\,. \tag{54}$$

with two Manley–Rowe constants of motion

$$I_{12a} = C_{1a}^2 - C_{2a}^2\,, \quad I_{ab} = C_{1a}^2 + 2C_b^2 + C_3^2\ . \tag{55}$$

and a new Hamiltonian

$$H_{\rm new} = 2Z_a \ln C_b + Z_b \ln\left(\frac{C_{2a} - C_{1a}}{C_{2a} + C_{1a}}\right)\,, \tag{56}$$

$$C_{1a} = \sqrt{I_{12a}}\cosh\alpha\,, \quad C_{2a} = \sqrt{I_{12a}}\sinh\alpha.$$

5.2 Star

A cluster of N triads, all connected *via* one common mode is called N-star cluster. Again, integrability of N-star depends on the types these connecting modes have in each triad of a cluster. NR-diagrams for all possible types of 3-stars are shown in Fig. 10. N-star cluster is the only known to us type

Figure 10: NR-diagrams for 3-star clusters. From right to left, from up to down: 3-star-A (three A-connections), 3-star-P (three P-connections), 3-star-1A-2P (one A-connection and two P-connections), 3-star-2A-1P (two A-connections and one P-connection)

of cluster for which an analytical study has been performed for *arbitrary* finite number N. The main idea can be briefly formulated as follows. N-star cluster has *2N+1* degrees of freedom, *N+1* Manley–Rowe constants of motion and one Hamiltonian, that is, we already have *N+2* independent first integrals in involution. To find $N-1$ additional integrals of motion, one can use construction of Lax operators, Painlevé analysis and irreducible forms, etc.; terminology used therein is pump and daughter wave for A- and P-mode correspondingly). The dynamical system, say for N-star-A, is regarded in the form

$$\dot{B}_{1j} = i\,\lambda_j B_3 \dot{B}_{2j}, \quad \dot{B}_{2j} = i\,\lambda_j B_3 \dot{B}_{1j}, \quad \dot{B}_3 = i\sum_{j=1}^{N} \lambda_j B_{1j} B_{2j}. \qquad (57)$$

Additional conservation laws found this way have necessarily *polynomial form*. The results for a generic N-star cluster are as follows: N-star-A (with all A-connections) and N-star-P (with all P-connections) are integrable for *arbitrary initial conditions* if $\lambda_j = 1/2$ or 1 or 2, examples of corresponding NR-diagrams shown in the Fig.10, for $N = 3$. N-star cluster with mixed A- and P-connections has no additional polynomial conservation laws. Complete set of additional polynomial conservation laws for integrable N-star cluster is omitted here for sake of place, and it can be found in [30]. Example for the case of AA-butterfly with $Z_a = 2\,Z_b$ reads

$$4(B_1B_2B_4^*B_5^* + B_1^*B_2^*B_4B_5)(B_1B_1^* + B_2B_2^*)$$
$$-2(B_3B_1^*B_2^* + B_3^*B_1B_2)^2 - [(B_1B_1^* + B_2B_2^*)^2 + 4B_1B_1^*B_2B_2^*](B_4B_4^* + B_5B_5^*).$$

However, most generic clusters demonstrate chaotic behavior and numerical investigations are unavoidable. The fact that our systems are Hamiltonian, allows us to perform numerical simulations based on the Hamiltonian expansion of the corresponding dynamical system and to construct Poincaré sections, example is in shown in the Fig.11 (chaotic evolution, simulations performed by F. Leyvraz 2008).

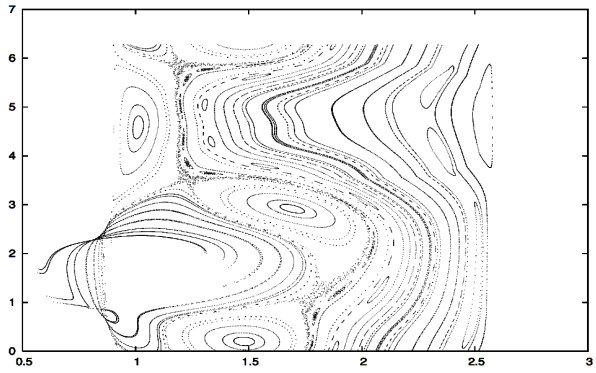

Figure 11: Example of Poincaré section for PP-butterfly with $Z_a/Z_b = 3/4$.

6 Coupling coefficient

As we have shown above, the integrability of a resonance cluster depends on the magnitude of the corresponding coupling coefficients. Expressions for coupling coefficients in *canonical variables* has been deduced for various types of wave systems possessing three-wave resonances: rotational capillary waves [6]; irrotational gravity-capillary waves [25]; drift waves [28], etc. They usually have a nice compact form, for instance, coupling coefficient V_{12}^3 for irrotational gravity-capillary water waves reads

$$\frac{(\omega_2^2 - \omega_2\omega_3 + \omega_3^2)}{\omega_1} k_1 - \omega_2 k_2 + \omega_3 k_3,$$

where $\omega = (g\,k + \sigma k^3)^{1/2}$ and g and σ are gravity acceleration and surface tension correspondingly. However, transformation of these expressions from the canonical to *physical variables* is not an easy task.

On the other hand, the application of multi-scale methods yields expressions for the coupling coefficients directly in physical variables. For instance,

coupling coefficients of the system of three resonantly interacting atmospheric planetary waves, with $\omega \sim m/[n(n+1)]$, have the form [18]

$$Z[n_2(n_2+1) - n_3(n_3+1)]/[n_1(n_1+1)], \tag{58}$$
$$Z[n_3(n_3+1) - n_1(n_1+1)]/[n_2(n_2+1)], \tag{59}$$
$$Z[n_2(n_2+1) - n_1(n_1+1)]/[n_3(n_3+1)], \tag{60}$$

with

$$Z = \int_{-\pi/2}^{\pi/2} [m_2 P^{(2)} \frac{d}{d\varphi} P^{(1)} - m_1 P^{(1)} \frac{d}{d\varphi} P^{(2)}] \frac{d}{d\varphi} P^{(3)} d\varphi.$$

Here two spherical space variables are the latitude φ, $-\pi/2 \leq \varphi \leq \pi/2$, and the longitude λ, $0 \leq \lambda \leq 2\pi$, and the notation $P^{(j)}$ is used for $P_{n_j}^{m_j}(\sin\varphi)$ which is the associated Legendre function of degree n_j and order m_j.

The multi-scale method is quite straightforward and can be programmed in some symbolical language [18]. However, only numerical magnitudes of the coupling coefficients have been computed for selected solutions of the resonance conditions, not an explicit algebraic formulas. The problem is due to some "bags" in *Mathematica* in computing integrals of the form

$$\int_0^{2\pi} \sin(mx)\sin(nx)dx, \quad \text{with} \quad m, n \in \mathbb{N}, \tag{61}$$

more discussion can be found in [18].

7 Summary

We have shown that in wave turbulent systems, usually described by statistical methods, some resonance clusters can generate regular patterns (elements of integrability in the terminology of F. Calogero) in k-space. The clusters can also demonstrate chaotic behavior depending on the form its NR-diagram, ratios of coupling coefficients and in some cases – on the initial conditions. Both type of cluster – with integrable and chaotic dynamics – do appear in real physical systems, e.g. [16] and [5] (atmospheric planetary and rotational capillary waves correspondingly). While performing sensible numerical simulations with resonance clusters, one of the most tedious and time-consuming parts of the corresponding simulations is the choice of initial conditions. A special procedure has been worked out (F. Leyvraz, 2008) that guarantees a uniform distribution of initial conditions according to Liouville measure, and assures as well that all conservation laws have the same value on each Poincaré section (example of computations in shown in Fig.11). However,

to trace effects due to the dynamical phases one has to use amplitude-phase representations.

Construction of resonance clustering and the set of corresponding NR-diagrams can also be used as a base of NR-reduced numerical models for numerical simulations with evolutionary dispersive nonlinear PDEs in cases when nonlinearity is small, [14].

Acknowledgements. The authors are very much obliged to the organizing committee of the workshop "INTEGRABLE SYSTEMS AND THE TRANSITION TO CHAOS II," who provided an excellent opportunity to meet and work together. They also highly appreciate the hospitality of Centro Internacional de Ciencias (Cuernavaca, Mexico), where part of the work was accomplished. Authors would like to thank A. Degasperis, S. Lombardi and F. Leyvraz for interesting and fruitful discussions. M.B. acknowledge the support of the Transnational Access Programme at RISC-Linz, funded by European Commission Framework 6 Programme for Integrated Infrastructures Initiatives under the project SCIEnce (Contract No. 026133). E.K. acknowledges the support of the Austrian Science Foundation (FWF) under project P20164-N18 "Discrete resonances in nonlinear wave systems".

References

[1] Arnold, V.I. *Geometrical Methods in the Theory of Ordinary Differential Equations.* (Springer, 1983)

[2] Bustamante, M.D., and E. Kartashova. *Europhys. Lett.* **85**: 14004 (2009)

[3] Bustamante, M.D., and E. Kartashova. *Europhys. Lett.* **85**: 34002 (2009)

[4] Calogero, F. In: V.E. Zakharov (ed.) *What is Integrability?*: 1 (Springer, 1991)

[5] Constantin, A., and E. Kartashova. *Europhys. Lett.* **86**: 29001 (2009)

[6] Constantin, A., E. Kartashova and E. Wahlén. E-print: arXiv:1001.1497 (2010)

[7] Eissa, M., W.A.A. El-Ganainia and Y.S. Hameda. *Physica A: Stat. Mech. Appl.* **356**(2-4): 341 (2005)

[8] Evans, N.W. Phys. Rev. A 41 (10): 5566 (1990)

[9] Haenggi, P. *ChemPhysChem* **3** (3): 285 (2002)

[10] Hasselmann, K. *Fluid Mech* **30**: 737 (1967)

[11] Kartashova, E. *Phys. Rev. Lett.* **72**: 2013 (1994); *AMS Transl. 2*: 95 (1998)

[12] Kartashova, E. *JETP Lett.* **83**(7): 341 (2006)

[13] Kartashova, E. *Europhys. Lett.* **87**: 44001 (2009)

[14] Kartashova, E. *Nonlinear Resonance Analysis: Theory, Computation, Applications* (Cambridge University Press, 2010, *in press*)

[15] Kartashova, E., and A. Kartashov. *Int. J. Mod. Phys. C* **17**(11): 1579 (2006); *Comm. Comp. Phys.* **2**(4): 783 (2007); *Physica A: Stat. Mech. Appl.* **380**: 66 (2007)

[16] Kartashova, E., and V.S. L'vov. *Phys. Rev. Lett.* **98**(19): 198501 (2007); *Europhys. Lett.* **83**: 50012 (2008)

[17] Kartashova, E., and G. Mayrhofer. *Physica A: Stat. Mech. Appl.* **385**: 527 (2007)

[18] Kartashova, E., C. Raab, Ch. Feurer, G. Mayrhofer and W. Schreiner. In: *Extreme Ocean Waves*: 97. Eds: E. Pelinovsky and Ch. Harif, (Springer, 2008)

[19] Karuzskii, A.L., A.N. Lykov, A.V. Perestoronin and A.I. Golovashkin. *Physica C: Superconductivity* **408-410**: 739 (2004)

[20] Lynch, P. In: *Large-Scale Atmosphere-Ocean Dynamics: Vol II: Geometric Methods and Models*: 64. Eds. J. Norbury and I. Roulstone (Cambridge University Press, 2002)

[21] Oliveira, H.P. de, I. Damia o Soares and E.V. Tonini *Cosmology and Astroparticle Physics*, doi: 10.1088/1475-7516/2006/02/015

[22] Kovriguine, D.A., and G.A. Maugin *Mathematical Problems in Engineering*, doi:10.1155/MPE/2006/76041 (2006)

[23] Kundu, M., and D. Bauer. *Phys. Rev. Lett.* **96**: 123401 (2006)

[24] Longuet-Higgins, M.S., and Gill, A.E. , Resonant interactions between planetary waves. *Proc. Roy. Soc. Lond.* **A299**, 120 (1967)

[25] McGoldrick, L.F. *Fluid Mech.* **21**: 305 (1967)

[26] Olver, P.J. *Applications of Lie groups to differential equations.* (Springer, 1993)

[27] Pedlosky, J. *Geophysical Fluid Dynamics.* Second Edition, (Springer, 1987)

[28] Piterbarg, L.I. AMS Trans. 2: 131 (1998)

[29] Tsytovich, V. N. *Nonlinear Effects in Plasma* (Plenum, New York, 1970).

[30] Verheest, F. *J. Phys. A: Math. Gen.* **21**: L545 (1988); *J. Math. Phys.* **29**: 2197 (1988)

[31] Zakharov, V.E., V.S. Lvov, and G. Falkovich. *Kolmogorov Spectra of Turbulence.* (Springer, 1992)

[32] Zakharov, V. E., A. O. Korotkevich, A. N. Pushkarev and A. I. Dyachenko. *JETP Lett.* **82** (2005), 487.